Archaeointensity of nineteenth-century Scottish firebricks from a foundry in Melbourne, Australia: comparisons with field models and magnetic observatory data



AGATHE LISÉ-PRONOVOST^{1,2*}, TOM MALLETT² & ANDY I. R. HERRIES²

¹School of Earth Sciences, University of Melbourne, Carlton, Victoria 3053, Australia

²The Australian Archaeomagnetism Laboratory, Department Archaeology and History, La Trobe University, Bundoora, Victoria, 3086, Australia

① AL-P, 0000-0002-7977-0512; TM, 0000-0002-7620-5075; AIRH, 0000-0002-2905-2002

*Correspondence: agathe.lise@unimelb.edu.au

Abstract: An archaeomagnetic intensity study was conducted on nineteenth-century firebricks manufactured in Scotland and used in an iron foundry in Melbourne, Australia, between 1842 and 1864 CE. Archaeointensity results obtained from bricks with a single component of magnetization gave values of 61.45 \pm 0.89 and 61.92 \pm 6.84 μT . These values are in agreement with historical absolute intensity measurements taken at the Melbourne geomagnetic observatory between 1858 and 1863 CE (61.17 \pm 0.078 μT) and with the gufm1 model based on mariners' data. A high-temperature vector component, presumably acquired at the time of manufacture in Scotland, was isolated in certain firebricks and an archaeointensity of 48.3 \pm 8.39 μT was obtained, which is consistent with the gufm1 model for Scotland at this time (48.79 μT). The dual archaeointensity record of the firebricks supports their geographical provenance, highlighting the potential for archaeointensity data to be used in archaeological artefact-sourcing studies, whilst anomalously high intensities recorded in one of the bricks highlight potential contamination issues from non-Earth magnetic fields in archaeometallurgical contexts. The new Melbourne archaeointensity data are the most precisely dated archaeomagnetic data produced so far for Australia.

There is a long-standing unbalance in archaeo- and palaeomagnetic data from the southern hemisphere relative to the northern hemisphere. New highquality empirical data from under-documented regions of the southern hemisphere are necessary to document complexities of the Earth's magnetic field and overcome the modelling limitations linked with unknown regional variability (e.g. Panovska et al. 2015; Constable et al. 2016). Progress has been made over the last decade in generating new archaeomagnetic data from South America (e.g. Hartmann et al. 2010; Goguitchaichvili et al. 2015; Poletti et al. 2016) and southern Africa (e.g. Neukirch et al. 2012; Tarduno et al. 2015; Hare et al. 2018). Along with these regions, Australia is the other major accessible southern hemisphere landmass and is yet to receive similar attention from the archaeomagnetic community, with the last archaeomagnetic study from Australia published 37 years ago. Yet, Australia has an outstanding potential for archaeomagnetic research given the long and extensive record of human occupation since at least 65 ka (Clarkson et al. 2017). Archaeomagnetic work in Australia is perhaps best known for the 'Lake Mungo excursion' that was suggested to be recorded in Aboriginal hearth features at Lake Mungo (Fig. 1) at c. 30 ka (Barbetti & McElhinny 1972, 1976). The validity of this event has since been discredited based on its lack of reproducibility and potential for sampling artefacts (Roberts 2008; Laj & Channell 2015). However, we note that re-dating of sediments surrounding the hearths show that these accumulated at 42–30 ka (Bowler et al. 2003) and thus the excursional data could potentially be associated with the Mono Lake (32 ka) or Laschamp (41 ka) excursions (Singer 2014).

In conjunction with the archaeomagnetic work at Lake Mungo, additional palaeodirections and absolute intensities were produced for late Pleistocene and Holocene SE Australia via Aboriginal fireplaces and burnt tree stumps (Barbetti 1973, 1977; Clark & Barbetti 1982; Barbetti et al. 1983) (Fig. 1). However, much of this work was not published in full, and the final archaeointensity dataset exists in the published record only as part of a single figure in Barbetti et al. (1983). Moreover, given that these

From: Tema, E., Di Chiara, A. & Herrero-Bervera, E. (eds) 2020. Geomagnetic Field Variations in the Past: New Data, Applications and Recent Advances. Geological Society, London, Special Publications, 497, 27–45. First published online January 16, 2020, https://doi.org/10.1144/SP497-2019-72

© 2020 The Author(s). Published by The Geological Society of London. All rights reserved.

For permissions: http://www.geolsoc.org.uk/permissions. Publishing disclaimer: www.geolsoc.org.uk/pub_ethics

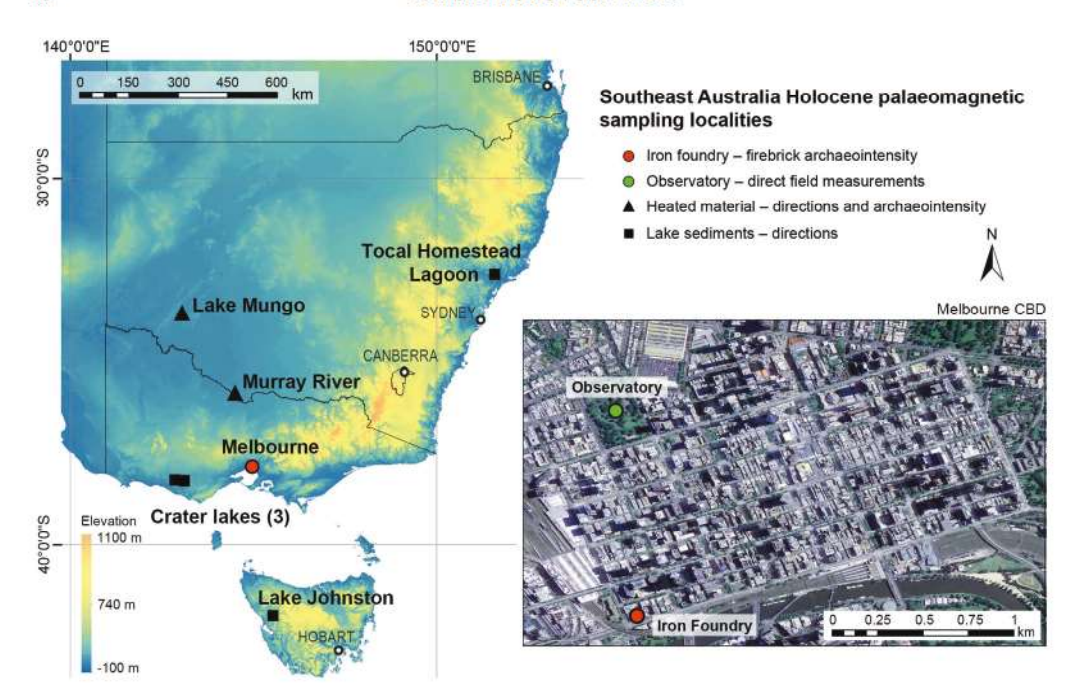


Fig. 1. Topographical map of SE Australia with the locations of the palaeomagnetic and archaeomagnetic study sites discussed in the text. Insert of Melbourne city centre showing the iron foundry site and the Flagstaff geomagnetic observatory, about 1 km in the distance.

measurements were made decades ago, most of the data were not treated with regular pTRM checks, nor corrections for differential cooling rates or anisotropy effects that are common in archaeological materials (e.g. Chauvin et al. 2000; Genevey et al. 2008; Poletti et al. 2016; Gómez-Paccard et al. 2019; Hervé et al. 2019). In modern studies, these treatments are deemed fundamental for paleointensity experiments, and data lacking these are now disregarded from modern data compilations (e.g. Poletti et al. 2018). Besides the archaeomagnetic work of Barbetti, previous Holocene palaeomagnetic field records from Australia consist of one full-vector palaeomagnetic record (relative palaeointensity and directions) from lake sediments in NE Australia (Constable 1985; Constable & McElhinny 1985), and four Holocene directional-only records from lakes and a lagoon in SE Australia (Barton & McElhinny 1981; Barton & Barbetti 1982; Anker et al. 2001; Gale et al. 2013) (Fig. 1). Thus, it is clear that new high-quality archaeomagnetic and palaeomagnetic data are required from a variety of archives to better constrain regional field variations in the Australian region, which will also contribute towards building archaeomagnetic reference curves as a dating tool for Australian archaeology and palaeoclimate research (e.g. Lisé-Pronovost et al. 2016).

Australian Holocene palaeointensity data in the GEOMAGIA50.v3 database (Brown et al. 2015)

include the Thellier-style experiments on baked archaeological materials, as reported in Barbetti et al. (1983) (Fig. 1). These data indicate a weak field from c. 6000 BP with a gradual rise until 4000-3000 BP, followed by a series of largeamplitude changes with maximum intensities at 2000 BP, 1200 BP (750 CE) and 400 BP (1550 CE). The Holocene relative palaeointensity record of Constable (1985) from NE Australia broadly follows the same trends but does not cover the historical period and the most recent c. 1500 years of large-amplitude changes, which are also not reflected in geomagnetic field models (e.g. SED3k.1, Korte et al. 2009; CALS3k.4, Korte & Constable 2011; pfm9k, Nilsson et al. 2014; HFM.OL1.AL1, Panovska et al. 2015; Constable et al. 2016). The most recent 400 years of geomagnetic field variability of these models are anchored or evaluated with the gufm1 historical model (Jackson et al. 2000), a massive compilation of geomagnetic measurements by mariners engaged in merchant and naval shipping. Such models and direct measurements are excellent to validate archaeomagnetic data where possible. Mariners at sea (the gufm1 model: Jackson et al. 2000) and scientists running the first magnetic observatories on the continent in the mid-nineteenth century provided the earliest direct measurements of the magnetic field in the Australian region, soon after Carl-Friedrich Gauss first developed the method in

1832 (Gauss 1833). Here we report on archaeointensity data derived from mid-nineteenth-century firebricks used in a Melbourne iron foundry and compare these data with unpublished absolute intensity measurements over the same period performed <1 km away at a historical magnetic observatory (Fig. 1). Building on an initial pilot study (Lisé-Pronovost *et al.* 2016), these constitute the first archaeomagnetic application to the continent's historical archaeological record.

Archaeological context and dating

The firebricks were sampled during archaeological salvage excavations in 2014 on a small c. 30 m² allotment at 556-560 Flinders Street, Melbourne, Australia, located in the city's central business district (Fig. 1) (Mallett et al. 2015; Lisé-Pronovost et al. 2016). The site preserved evidence of several different occupation phases dating to soon after the colonial city's establishment in 1835. These include early industrial works from 1842-64, and later retail and commercial operations post-1864 and into the twentieth century. The firebricks were derived from the industrial phase of site use, where the allotment formed part of larger factory grounds associated with 'Langland's Iron Foundry', Melbourne's first early- to mid-nineteenth-century engineering firm (Myers et al. 2018). The bricks were sampled unorientated from a secondary fill deposit within a handmade-brick-lined well (Fig. 2a), which was capped with iron slag deposited as a thick layer across much of the site towards the end of the industrial foundry phase (Mallett et al. 2015). The capping slag and underlying foundry occupation and pre-foundry surfaces were subsequently cut for the placement of new building foundations on the allotment in 1864, constraining the age of the fill deposit, and thus brick use, to between 1842 and 1864 (Mallett et al. 2015).

The firebricks themselves were manufactured in Scotland and imported to Melbourne during the foundry phase of occupation. FBW-1 and FBW-2 (Fig. 2b) were both manufactured in Tranent, East Lothian, Scotland, by 'John Grieve Bank Park Firebrick Works' (1860-93) as ascertained from the brick stamp (Douglas et al. 1985). As such, these bricks must have been used in Melbourne some time between 1860 and 1864 towards the end of the iron foundry phase. FBG (Fig. 2b) was manufactured by 'Garnkirk Fire Clay Co.' (stamped: 'Garnkirk Warranted', 'Patent') from 1837 to 1901 in Lanarkshire, Scotland (Douglas et al. 1985). Thus, according to archaeological context, it must have been used in Melbourne some time between 1842 and 1864, although the brick may have been fired in Scotland any time between 1837 and 1864. In a pilot thermal demagnetization study,

Lisé-Pronovost et al. (2016) demonstrated that a proportion of samples exhibited a single-component thermoremanent magnetization (TRM), indicating that they were likely to have been heated to high temperatures, overprinting any TRM formed by their manufacture in Scotland. However, others showed distinct dual-remanence components, suggesting that they were subject to lower heating temperatures in Australia and potentially preserve their original manufacturing TRM from Scotland. The firebricks themselves exhibit some visual evidence of heating, which was also reflected in much of the pilot archaeomagnetic data. As the firebricks were not sampled from in situ foundry features (e.g. a kiln), however, the exact way they were heated and used in Australia is unknown.

Firebrick manufacture

Firebricks were produced following the Industrial Revolution out of an increasing need for refractory materials that could withstand extreme temperatures and stress associated with process and manufacturing industries. Their production in the UK during the nineteenth century was largely centred in the midland belt of Scotland, with 'fireclays' extracted from coal-bearing deposits within the Carboniferous-aged Millstone Grit Series (Douglass & Oglethorpe 1993). Fireclays are classed as aluminosilicates with up to c. 90% of their mineral assemblage dominated by disordered kaolinite, hydrous mica and quartz, along with minor inclusions of chlorite, carbonaceous matter and iron such as siderite (Highley 1982). Their refractory properties are due to a high aluminium-oxide content and lower proportions of mica, with historical firebricks reported to contain c. 28-43% Al₂O₃ (Sanderson 1990). Douglass & Oglethorpe (1993) provide details on the manufacturing process of firebricks in nineteenth-century Scotland: following extraction, the fireclay raw material was broken down in a crushing machine and transferred to dry pan mills. Then 10-15% of 'grog' (burnt brick and clay) was added to the raw fireclays to reduce shrinkage during firing and drying. After mixing and adding water to aid plasticity, materials were transferred into brick machines for moulding and dried or semi-dried on heated floors before being placed into firing kilns.

Melbourne Magnetic Observatory

Scientific measurements of the magnetic field in Melbourne were made by Georg Neumayer at the Flagstaff Observatory (now the Flagstaff Gardens: Fig. 1) between January 1858 and September 1862, and then at the new nearby Melbourne Observatory from September 1862 until February 1863

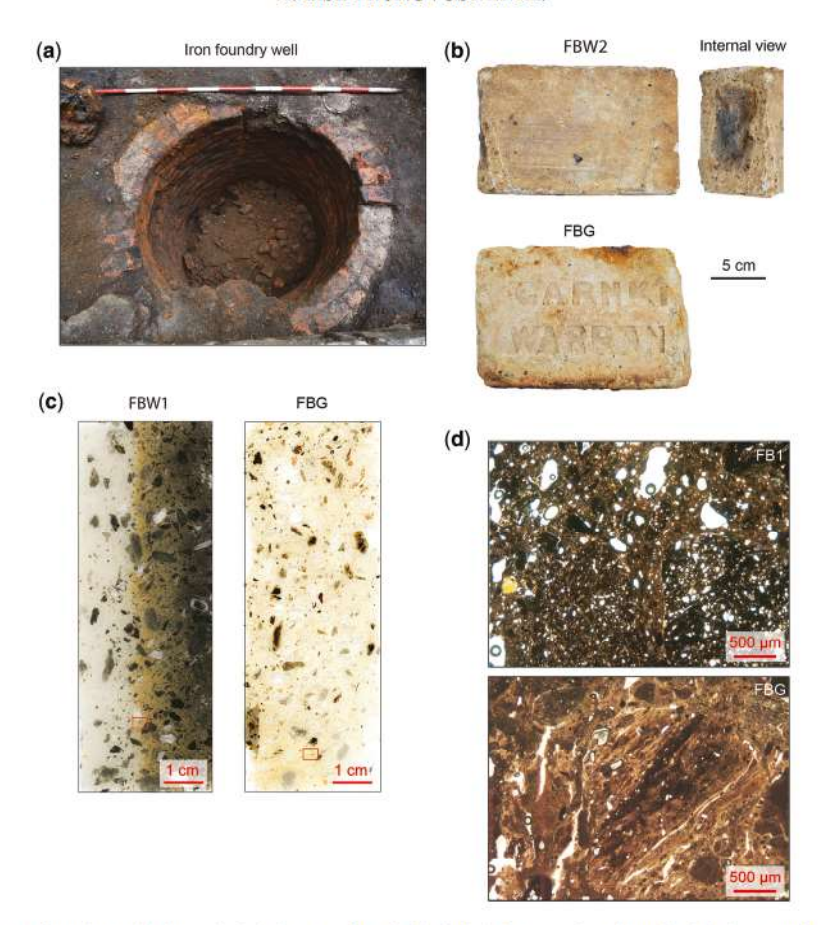


Fig. 2. (a) Iron foundry well where the bricks were found; (b) firebricks FBW-2 and FBG with the manufacture stamp, and the internal view of brick FBW-2 with dark inner portion and light outer portion; (c) thin sections of the bricks (vertical along the samples' Z axis) showing a distinct colour change between interior and exterior in FBW-1; and (d) magnified region of thin sections showing the difference in the fabrics of the bricks made by different manufacturers.

(Neumayer 1867). Magnetic directions were measured hourly and the absolute horizontal force was measured monthly. Estimates of total field (F) values are derived from the measured horizontal force (H) and inclination (I) values using the equation: $F = H/\cos(I)$. The monthly total intensity data over the 5 year period (1858–63) exhibits a monotonic straight-line decreasing secular variation from 61.28 to 61.07 μ T, with an average value of 61.17 \pm 0.078 μ T.

Methods

Sample preparation

The firebricks were prepared for magnetic and palaeointensity experiments at The Australian

Archaeomagnetism Laboratory, La Trobe University in Melbourne, Australia. The bricks were drilled into 22 mm diameter cylinder cores using a water-cooled bench drill from the stretcher side of the brick to preserve historical brick stamps located on their main flat face (Fig. 2b). The cores were then cut into 25 mm sample sections, which provide a transect of magnetic properties from one side of the brick to the other. For this study, a total of 58 samples were analysed. Six samples per brick underwent archaeointensity experiments (FBW-1-A1, FBW-1-A4, FBW-1-C4, FBW-1-C5, FBW-1-D4, FBW-1-D5; FBW-2-B1, FBW-2-B2, FBW-2-C1, FBW-2-C2, FBW-2-C4, FBW-2-C5; FBG-C1, FBG-C2, FBG-C3, FBG-C4, FBG-C5, FBG-D1). Six or more samples per brick were used for thermal and alternating field demagnetization, six fresh samples for cooling-rate experiments, and 12 samples

were used for further rock magnetic analysis. Thin sections were taken from the bricks to look at fabric differences and inclusions (Fig. 2c, d).

Magnetic analysis

Magnetic susceptibility, alternating field and thermal demagnetization data were acquired at The Australian Archaeomagnetism Laboratory, La Trobe University, in order to characterize the magnetic mineral assemblage. Mass-specific magnetic susceptibility was measured at low field (χ_{LF}: 0.465 kHz) using a Bartington MS2 sensor prior to heating, and after each thermal demagnetization step to assess for magnetomineralogical alteration. Alternating field demagnetization was undertaken up to 80 mT in 29 steps with an Advanced Geoscience Instruments Co. (AGICO) LDA5 Alternating Field Demagnetizer. Thermal demagnetization experiments conducted using a 30-33 step protocol from 0 to 700°C using a shielded Magnetic Measurements MMTD80a Thermal Demagnetizer in a zero-field cage. Remanence measurements were taken using an AGICO JR-6 Spinner Magnetometer (2.4 µA m⁻ sensitivity) and demagnetization data were processed using PuffinPlot 1.03 (Lurcock & Wilson 2012). In order to precisely characterize the magnetic remanence carriers, hysteresis loops, backfield curves and first-order reversal curves (FORCs) were measured at room temperature using a Princetown Measurements MicroMag Vibrating Sample Magnetometer at the Australian National University Paleomagnetism Laboratory and at the Institute for Rock Magnetism, University of Minnesota, USA. Backfield curves were deconvoluted using the MAX UnMix web application (Maxbauer et al. 2016) and FORCs were processed in FORCinel 3.06 (Harrison & Feinberg 2008) using VARIFORC smoothing (Egli 2013).

Archaeointensity experiment

The IZZI variant of the Thellier protocol (Yu & Tauxe 2005) was used, with in-field and zero-field pTRM checks (Thellier & Thellier 1959; Coe 1967; Riisager & Riisager 2001) to detect magnetomineralogical changes. The archaeointensity experiment included 18 heating steps to 100, 200, 225, 250, 275, 300, 325, 350, 375, 400, 425, 450, 475, 500, 525, 550, 575 and 600°C. An applied field of 60 μT was generated for in-field steps using a power supply EL301R plugged into the MMTD80a thermal demagnetizer furnace, with remanence measurements taken on the JR-6 spinner magnetometer. Also included in the dataset are two samples from the pilot study for which a 12-step experiment and 40 μT field were used (FBW-1-A1 and FBW-1-A4: Lisé-Pronovost et al. 2016). χ_{LF} measurements were taken during the experiment to monitor for magnetomineralogical alteration. The program ThellierTool 4.22 and its default class criteria were used for data analysis (Leonhardt et al. 2004a), and the built-in correction for magnetomineralogical alteration was applied (Valet et al. 1996). The correction uses the cumulative alteration differences between pTRM values and pTRM checks for a given interval. The alteration criteria include d(CK), which is the difference between pTRM-check and related pTRM acquisition normalized to TRM, and d(pal), which is the ratio of uncorrected to corrected archaeointensity normalized to the uncorrected value (values shown in Tables 1 and 2) (Leonhardt et al. 2004a).

Archaeological artefacts, such as bricks, tiles and ceramics, can have magnetic anisotropy that impact the archaeointensity results (Rogers et al. 1979; Veitch et al. 1984; Chauvin et al. 2000; Genevey et al. 2008). The anisotropy of thermal remanent magnetization (ATRM) was measured in six directions (+Z, -Z, +X, -X, +Y, -Y) for each sample to evaluate and correct for the effect of magnetic anisotropy on the archaeointensity data. The Z direction was re-measured as a final step to check for alteration. The experiment was repeated at temperatures of 350 and 500°C in order to allow for selection of the most appropriate ATRM correction per sample, with a natural remnant magnetization (NRM) fraction of >30% and avoiding further alterations by repeated heating. The anisotropy correction factor (FATRM) was calculated according to Veitch et al. (1984) using the Matlab code of Tema et al. (2015). Fresh samples from FBW-1 and FBW-2 were also measured to evaluate the possible effect of magnetomineral changes during the archaeointensity experiment on the FATRM.

The cooling rate is also known to impact archaeointensity results because the laboratory fan-forced cooling is typically much faster than the original archaeological cooling when the ancient field was recorded (Fox & Aitken 1980; Hervé et al. 2019). The original cooling rate of the firebricks FBW and FBG is unknown; however, rapid laboratory cooling is known to overestimate the ancient field, and cooling-rate correction factors can be calculated with laboratory slow cooling (e.g. Genevey et al. 2008). Cooling-rate experiments were performed on fresh samples following the method of Hartmann et al. (2010) (see also Genevey et al. 2008; Genevey & Gallet 2002) at the Paleomagnetism Laboratory at the Australian National University, using an ASC TD48 oven with in-house cooling-rate control. A different oven was used because the oven at TAAL does not allow cooling-rates experiments, and the same applied field of 60 µT was set and monitored in both ovens. Two fresh samples per brick were measured at a rapid cooling rate (fan on, about 0.5-1 h; pTRMr1), slow cooling rate (0.8°C/min; pTRMs), and a second rapid (pTRMr2) cooling rate at 350 and 500°C. Alteration is calculated

Table 1. Archaeointensity results for the low-temperature component (M2) acquired in the iron foundry in Melbourne, Australia

FBW-1	Regular A1 A4-M2 C4-M2 C5 D4 D5 Average SD MMC-cor A1 A4-M2	61.92 66.41 63.13 61.16 61.49 60.63 62.46 2.11	0.99 4.73 0.85 0.55 0.77 0.64	A B A A	0.00	480.00	9.00	0.76				
	A4-M2 C4-M2 C5 D4 D5 Average SD MMC-con	66.41 63.13 61.16 61.49 60.63 62.46	4.73 0.85 0.55 0.77	B A	0.00		9.00	0.76				
	C4-M2 C5 D4 D5 Average SD MMC-con	63.13 61.16 61.49 60.63 62.46	0.85 0.55 0.77	A			7.00	0.76	0.83	39.50	2.00	0.70
	C5 D4 D5 Average SD MMC-con	61.16 61.49 60.63 62.46	0.55 0.77		100 00	350.00	6.00	0.87	0.75	9.20	3.70	7.40
	C5 D4 D5 Average SD MMC-con	61.16 61.49 60.63 62.46	0.55 0.77		100.00	475.00	13.00	0.93	0.89	61.30	1.30	1.10
	D4 D5 Average SD MMC-con A1	61.49 60.63 62.46	0.77		100.00	525.00	15.00	0.74	0.89	73.20	1.30	1.00
	D5 Average SD MMC-cor A1	60.63 62.46		A	100.00	525.00	15.00	0.60	0.92	44.00	1.90	0.30
	Average SD MMC-con A1	62.46	0.01	A	0.00	575.00	18.00	0.91	0.92	79.50	3.50	2.50
	MMC-cor			**	0.00	575.00	10.00	0.71	0.72	17.50	5.50	2.50
	A1											
		rected										
	A 4 M/2	61.46	0.96	A*	0.00	480.00	9.00	0.75	0.83	39.90	NA	NA
	714-IVIZ	61.50	3.97	B*	0.00	350.00	6.00	0.87	0.75	10.10	NA	NA
	C4-M2	63.22	1.00	A*	100.00	425.00	11.00	0.86	0.88	47.70	NA	NA
	C5	60.70	0.78	A*	0.00	575.00	18.00	0.89	0.91	63.40	NA	NA
	D4	62.15	0.93	A*	100.00	575.00	17.00	0.70	0.93	43.90	NA	NA
	D5	61.83	0.58	A*	0.00	600.00	19.00	0.93	0.93	93.00	NA	NA
	Average	61.81	0.50	Α	0.00	000.00	17.00	0.75	0.75	25.00	11/1	III
	SD	0.84										
FBW-2	Regular											
	B1-M2	75.46	1.28	A	0.00	350.00	9.00	0.98	0.65	37.80	2.00	2.00
	B2-M2	72.02	0.67	A	0.00	400.00	11.00	0.94	0.86	87.70	2.10	3.00
	C1-M2	73.50	0.81	A	0.00	375.00	10.00	0.97	0.74	64.80	0.70	1.60
	C2-M2	68.41	0.62	A	100.00	400.00	10.00	0.88	0.86	82.70	1.10	2.30
	C4	59.56	0.63	A	275.00	575.00	13.00	0.71	0.91	61.20	2.90	4.00
	C5	63.23	0.70	A	0.00	575.00	18.00	0.97	0.92	81.10	3.40	3.80
	Average	68.70	0.79	Α	0.00	373.00	10.00	0.57	0.52	01.10	3.40	3.00
	SD	6.22	0.79									
	MMC-cor	rected										
	B1-M2	73.94	1.17	A*	0.00	350.00	9.00	0.99	0.65	40.70	NA	NA
	B2-M2	74.19	0.89	A*	0.00	400.00	11.00	0.93	0.86	67.20	NA	NA
	C1-M2	74.70	0.94	A*	0.00	375.00	10.00	0.97	0.74	57.20	NA	NA
	C2-M2	69.47	0.85	A*	0.00	400.00	11.00	0.90	0.86	63.60	NA	NA
	C4	64.46	1.01	A*	0.00	600.00	19.00	0.93	0.94	56.00	NA	NA
	C5	65.36	0.72	A*	0.00	600.00	19.00	0.99	0.92	82.90	NA	NA
	Average	70.35	0.93	A	0.00	000.00	17.00	0.77	0.72	02.70	1111	11/1
	SD	4.62	0.55									
FBG	Regular											
	C1	NA	NA	C	NA	NA	NA	NA	NA	NA	NA	NA
	C2	60.55	1.04	В	0.00	600.00	19.00	0.84	0.92	45.40	5.20	7.20
	C3	61.06	1.39	A	0.00	600.00	18.00	0.95	0.52	21.60	4.30	0.20
	C4	69.38	1.55	A	200.00	600.00	17.00	0.52	0.90	21.00	3.50	4.60
	C5	68.68	2.18	A	250.00	600.00	15.00	0.57	0.89	15.80	4.50	4.90
	D1	64.05	0.92	A	200.00	600.00	17.00	0.72	0.93	47.20	2.60	3.40
	Average	64.74	0.72	А	200.00	000.00	17.00	0.72	0.75	47.20	2.00	3.40
	SD	4.14										
	MMC-cor											
	C1 [†]	78.69	0.98	B*	250.00	600.00	15.00	0.44	0.91	32.20	NA	NA
	C2	56.22	1.77	A*	0.00	600.00	19.00	0.81	0.92	23.70	NA	NA
	C3	60.93	1.77	A*	0.00	600.00	18.00	0.93	0.51	16.60	NA	NA
	C4	63.53	1.64	A*	0.00	600.00	19.00	0.89	0.84	28.90	NA	NA
	C5	59.12	1.89	A*	0.00	575.00	18.00	0.89	0.88	24.70	NA	NA
	D1	57.76	0.83	A*	0.00	525.00	16.00	0.71	0.91	45.20	NA	NA
	Average	59.51	0.00		5.00	525.00	10.00	W. / I			18000	
	SD	2.84										

Average palaeointensity estimate and standard deviation are calculated for class A and B samples. Class C is unsuccessful.* indicates the class after magnetomineral change (MMC) correction (Valet et al. 1996).

Figurificantly higher PI value. Not used in average and standard deviation (SD) calculation; N, is the number of successive points in linear fragment; f, is the fraction of NRM; g, is the gap factor; g, is the quality factor; d (pal), is the ratio of uncorrected to corrected archaeointensity normalized to the uncorrected value; d(ck), is the difference between pTRM-check and related pTRM acquisition normalized to TRM.

Table 2. Archaeointensity results for the high-temperature component (pM1) presumably acquired at the time of manufacture in Scotland

Brick	Sample	H (μT)	SD	Class	T _{min} (°C)	T _{max} (°C)	N	f	8	q	d (pal)	d (ck)
FBW-1	Regular											,
	A4-pM1	17.18	3.11	C	440	580	6	0.22	0.65	0.8	8.1	82.7
	C4-pM1	24.26	6.09	C	525	600	4	0.16	0.49	0.3	6.5	28
	MMC-corrected											
	A4-pM1	31.39	12.5	C*	440	580	6	0.15	0.57	0.2	NA	NA
	C4-pM1	31.07	14.08	C*	525	600	4	0.14	0.56	0.2	NA	NA
FBW-2	Regular											
	B1-pM1	50.19	4.38	C	400	575	8	0.52	0.72	4.3	46.4	35.5
	B2-pM1	37.67	2.52	C	450	600	7	0.25	0.79	2.9	59.4	28.8
	C1-pM1	37.76	2.31	C	425	575	7	0.23	0.76	2.9	3.3	19.1
	C2-pM1	30.28	1.99	C	450	600	7	0.25	0.81	3.1	59.2	32
FBW-2	MMC-corrected											
	B1-pM1	54.71	8.1	B*	400	600	9	0.98	0.77	5.1	NA	NA
	B2-pM1	48.52	3.07	B*	450	600	7	0.59	0.8	7.5	NA	NA
	C1-pM1	44.98	3.62	C*	425	575	7	0.2	0.79	2	NA	NA
	C2-pM1	39.99	2.64	A*	450	600	7	0.6	0.82	7.4	NA	NA
	Average SD	47.74 7.39										

Average palaeointensity estimate and standard deviation are calculated for class A and B samples. Class C is unsuccessful. *indicates class after magnetomineral change (MMC) correction (Valet et al. 1996).

N, is the number of successive points in linear fragment; f, is the fraction of NRM; g, is the gap factor; q, is the quality factor; d(pal), is the ratio of uncorrected to corrected archaeointensity normalized to the uncorrected value; d(ck), is the difference between pTRM-check and related pTRM acquisition normalized to TRM.

using the equation: $100 \times (pTRMr1 - pTRMr2)/pTRMr1$. The sample with the least alteration per brick is used to calculate the cooling-rate correction factor using the equation: $100 \times (pTRMr1 + pTRMr2)/2/pTRMs)$.

The firebricks FBW-1 and FBW-2 have two vector components of magnetization on one of their sides (Lisé-Pronovost et al. 2016). An archaeointensity estimate can be calculated for each component following the two-step method of Yu & Dunlop (2002) (Fig. 2). The first step is to identify the remagnetization temperature (T^*) at the vector junction. The second step is to subtract the high-temperature vector pM1 from the low-temperature vector M2. pM1 is the vector remaining from the initial M1 (acquired during brick manufacture) after a subsequent heating to T*. pM1 is subtracted from each following the thermal demagnetization step $(T_i < T^*)$ to obtain adjusted M2 values (M2*). This allows two separate Arai plots and palaeointensity estimates per sample (pM1 and M2*: Fig. 3).

Results

Magnetic mineral assemblage

The magnetic mineralogy of samples from brick FBG are relatively uniform and are characterized

by an average χ value of $229 \times 10^{-8} \,\mathrm{m}^3 \,\mathrm{kg}^{-1}$. Wasp-waisted hysteresis loops (Fig. 4a) indicate the presence of at least two contrasting coercivities. The high-coercivity portion is reflected by about 40% of the NRM remaining after alternating field demagnetization at 80 mT (Fig. 4c). Thermal demagnetization of the FBG subsamples shows that the main remanence unblocks at between 560 and 580°C (and up to 600°C), indicating that phases of magnetite or oxidized magnetite dominate the NRM (Fig. 4b). A minor portion of NRM remains until c. 660-680°C, which is likely to relate to the high-coercivity mineral hematite, whilst a small inflection is also observed at lower temperatures of c. 140–240°C, which possibly relate to Ti-substituted, oxidized or epsilon iron oxides (Dunlop & Özdemir 1997; López-Sanchez et al. 2017). The orthogonal projections are single component and somewhat noisy (Fig. 5e, f), probably due to their friable texture that may have slightly altered the directional data. FBG has a homogenous fabric across the brick, showing no colour variation (Fig. 2b, d). However, the reuse of broken bricks with a similar sand temper to FBW (see details below) can be identified as distinct clasts within the brick.

Mineral magnetic data from bricks FBW-1 and FBW-2 exhibit greater variability because each brick comprises two different types of

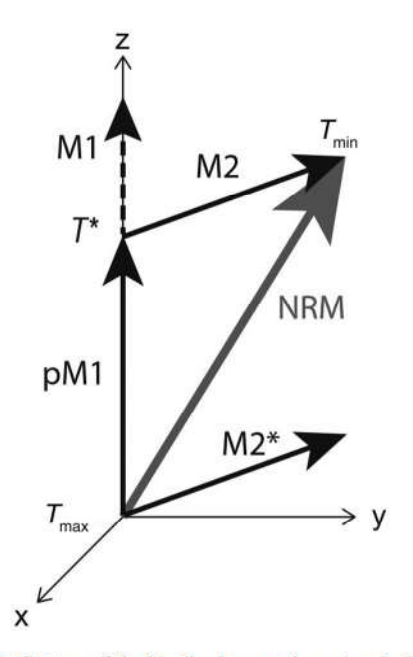


Fig. 3. Cartoon of the idealized magnetic vectors in the firebrick. NRM is the natural remanent magnetization; M1 is the thermal remanence acquired during the brick manufacture in Scotland; pM1 is the remaining high-temperature remanence after a subsequent lower-temperature heating event M2 in Australia; and M2* is the adjusted vector used for the Arai plot palaeointensity estimation. Archaeointensity estimates can be calculated for pM1 and M2* following the method of Yu & Dunlop (2002).

material: a darker inner section and a white outer section (Fig. 2b, d). This internal difference is likely to arise from purposeful non-homogeneous material being used for the brick manufacture (Douglass & Oglethorpe 1993), Thin-section observations support the manufacture details (cf. see the 'Firebrick manufacture' section) and reveal that the interior of the FBW bricks has a fine-grained sand temper with a high proportion of organic charcoal/plant remains with void spaces created by their burning during heating. In contrast, the exterior of the brick has a larger proportion of coarser-grained sand temper without organics. The light FBW samples have an average χ value of 371 \times 10⁻⁸ m³ kg⁻¹. These values are comparable in magnitude to those of FBG, which is composed of similar light fireclays. Also similar to FBG, the light-coloured exteriors of the FBW bricks have slightly wasp-waisted hysteresis loops and higher proportions of NRM remaining after AF demagnetization at 80 mT, compared to the dark sections (Fig. 4c). In contrast, the dark interior sections have a higher average χ value $(1314 \times 10^{-8} \text{ m}^3 \text{ kg}^{-1})$, higher remanence values (Figs 4a & 5) and pot-bellied hysteresis loops with

very little high-field contribution, indicating the saturation of most minerals in fields of 1 T (Fig. 4a). Thermal demagnetization data show that the main portion of NRM is removed at 620-660°C for the dark inner portion, and at a lower unblocking temperature in the outer light portion of 520-560°C, with a significant drop in remanence occurring at lower temperatures (terminating at c. 240-400°C) in most samples. Magnetomineralogical alteration during heating is observed in some samples to varying degrees at temperatures ranging from 200 to 700°C (Fig. 5). There is no apparent link between the magnetic mineralogy of a sample and its single- or doublevector component (Fig. 5), suggesting that it relates to brick usage in the iron foundry and not the magnetic mineralogy (Lisé-Pronovost et al. 2016).

Given the complex mineralogy of the FBW bricks, FORC analysis (FORCinel: Harrison & Feinberg 2008) and back-curve unmixing (MaxUnmix: Maxbauer et al. 2016) were conducted (Fig. 6). Four magnetic mineral components were identified: low (C1), intermediate (C2 and C3) and high (C4) coercivities (Fig. 6). There are two main differences between the dark and light portions. The first is an additional contribution of intermediate coercivity C3 in the dark inner portion (proportion of 46% for FBW-2 dark), which is absent in the light portion. The second is the greater proportion of the high magnetic coercivity component C4 in the light outer portion (proportion of 18% in FBW-2 light and 1% in FBW-2 dark: Fig. 6b). The FORC diagrams of both the light and dark portions are, nevertheless, similar, and include a prominent single to vortex domain (SD) signature with closed contours distributed along the central ridge and a negative feature along the Bu axis (Roberts et al. 2014). These are likely to relate to the dominant intermediate coercivity components (C2 and C3: Fig. 6) and indicate excellent magnetic remanence recorders. The lowest coercivity C1 (9 mT for a dark subsample; 28 mT for a light subsample) must reflect a smaller proportion of finer magnetic grains given the central ridge's intersection with the Bu axis (as opposed to MD grains, which spread along the Bu axis: Roberts et al. 2014).

Archaeointensity

The archaeointensity results for the low-temperature vector M2 (Fig. 3) acquired in Melbourne are reported in Table 1. The majority of samples are class A, except for three samples identified by ThellierTool default criteria to have undergone magnetomineralogical alteration during heating (FBW-1-A-M2, class B; FBG-C1, class C; FBG-C2, class B). Only one of the 18 samples is of class C (unsuccessful), which represents a success

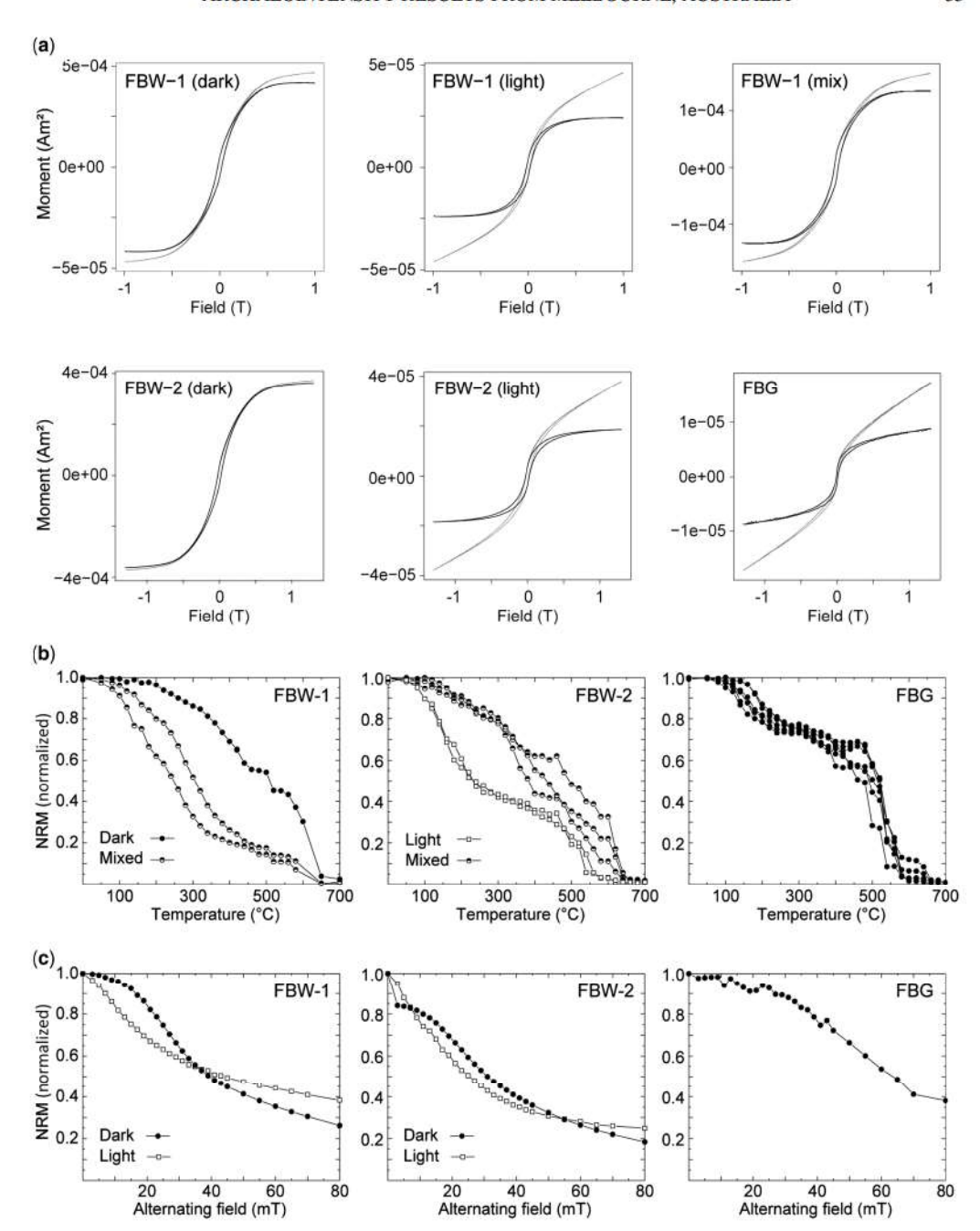


Fig. 4. Magnetic mineralogy of the firebricks. Representative (a) hysteresis loops (grey) and corrected for high-field contribution (black), (b) thermal demagnetization plots with magnetic susceptibility measured after each heating step and (c) stepwise alternating field demagnetization plots.

rate of 94%. The class C sample from the exterior of FBG-C1 has distinctively higher magnetic susceptibility and archaeointensity values ($78.06 \mu T$). An iron slag stain visible on the sample is likely to

account for this higher value and was therefore excluded from the average calculations. The average regular archaeointensity values per brick are 62.46 \pm 2.11 μ T (FBW-1: six samples), 68.7 \pm 6.22 μ T

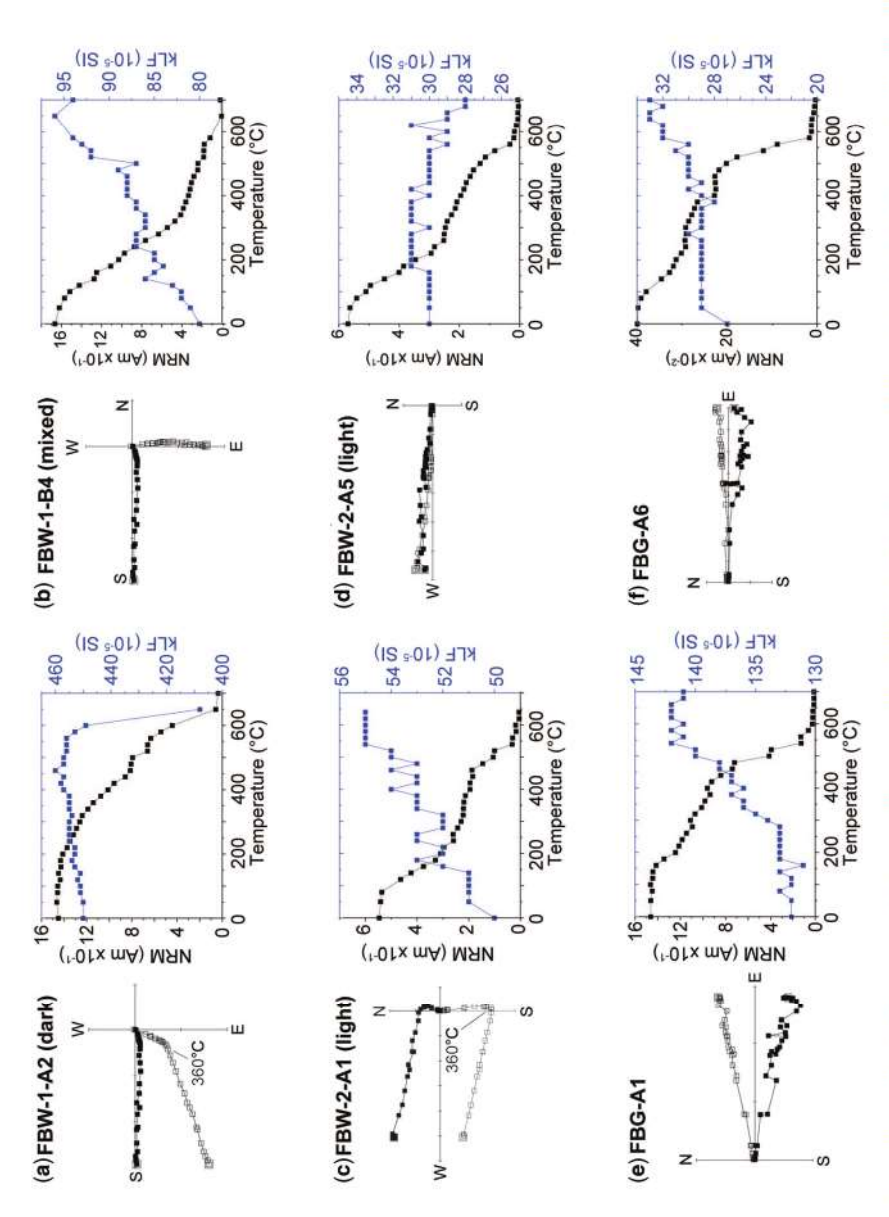


Fig. 5. Orthogonal projection and thermal demagnetization plot with magnetic susceptibility measured after each heating step as a proxy for magnetomineralogical alteration, for representative samples of bricks (a) & (b) FBW-1, (c) & (d) FBW-2 and (e) & (f) FBG. All bricks have a single component aligned to the origin, and bricks FBW-1 and FBW-2 also have samples with two directional components of magnetization. Note the different magnetic susceptibility axis ranges for each plot.

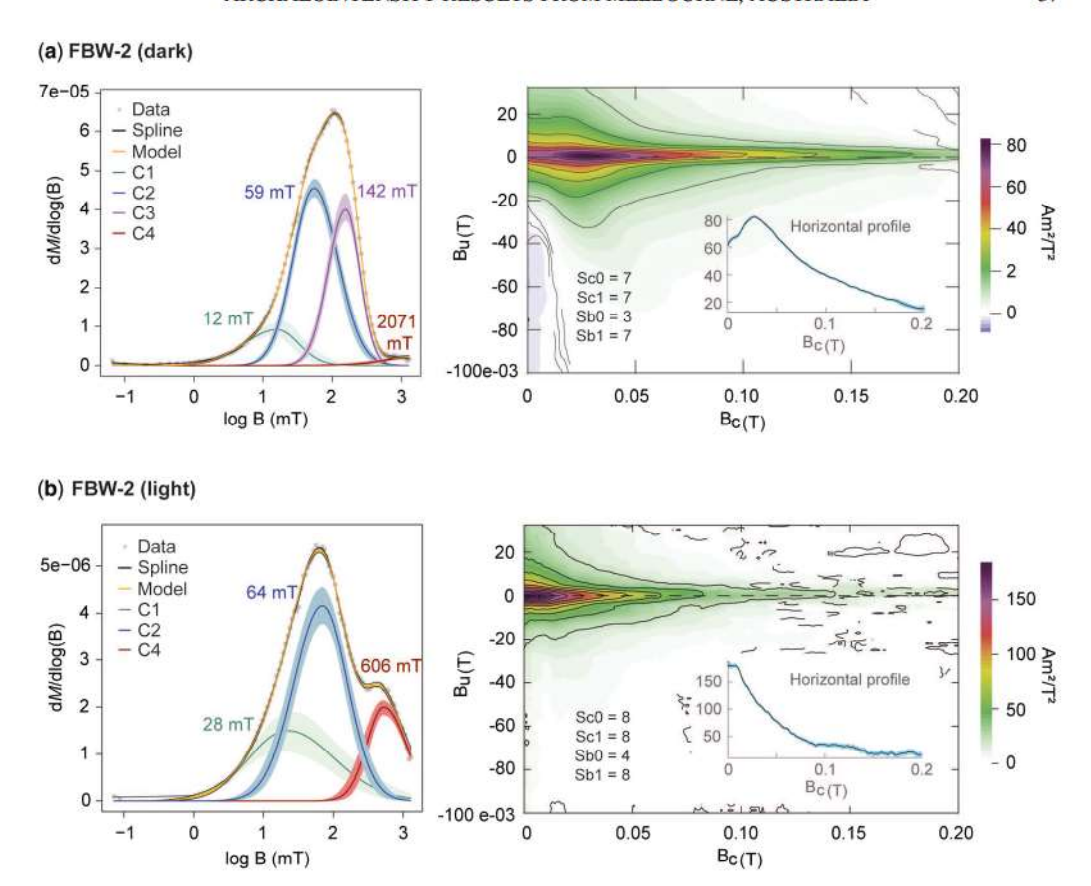
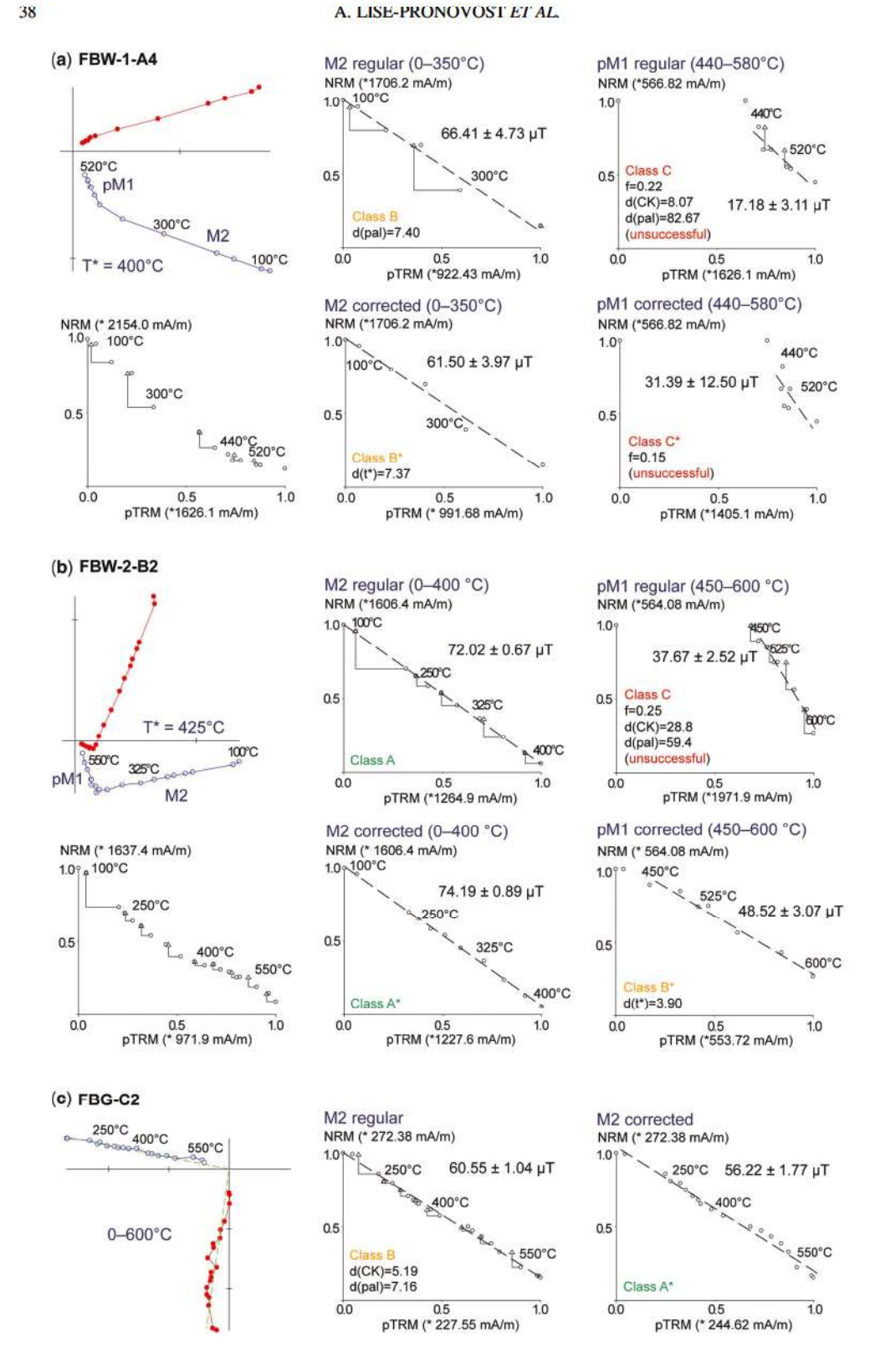


Fig. 6. Magnetic mineral difference between the dark (inner) and light (outer) part of the firebricks FBW-1 and FBW-2 (same sample as in Fig. 4a 'FBW-2 dark' and 'FBW-2 light'). Back-curve coercivity unmix components (MaxUnumix: Maxbauer *et al.* 2016) and first-order reversal curve diagram (FORCinel: Harrison & Feinberg 2008) for representative samples of (a) the dark (inner) part and (b) the light (outer) part.

(FBW-2: six samples) and $64.74 \pm 4.14 \,\mu\text{T}$ (FBG: five samples). The magnetic mineralogy of the bricks indicates no multidomain particles (Fig. 6), which fulfills the fundamental criteria for applying the magnetomineralogical change (MMC) correction built into the ThellierTool (Valet et al. 1996; Leonhardt et al. 2004b). Applying the correction of Valet et al. (1996) upgrades the aforementioned samples that underwent magnetomineralogical changes to classes B and A (e.g. FBG-C2: Fig. 7c). Applying the correction to all samples returns slightly higher standard deviations of archaeointensity estimates per sample but a more precise archaeointensity estimate (lower standard deviation) per brick (Tables 1 and 2). This ameliorated precision possibly relates to the complex magnetic mineralogy and the variable alterations that occurs within one brick (Fig. 6), as also indicated by the d(pal) and d(CK) values often being near the cutoff values for class A (5, 5) and B (7, 10) (Table 1). The correction is thus considered to advantageously account for subtle magnetomineralogical changes within a brick and to provide more precise archaeointensity estimates per brick. The average MMC-corrected archaeointensity values are $61.81 \pm 0.84 \,\mu\text{T}$ (FBW-1: six samples), $70.35 \pm$ 4.62 μ T (FBW-2: six samples) and 59.51 \pm 2.84 μ T (FBG: five samples) (Table 1; Fig. 8). The magnetic anisotropy (ATRM) and cooling-rate (cool)corrected archaeointensity values for the experiments at 350°C are presented in Table 3 and Figure 8. The 350°C experiment is selected because of a sufficient NRM fraction (average 50 ± 14%, ranging from 30 to 82%) and negligible alteration (<3%). The average anisotropy correction factor (ATRM) is 1.01 ± 0.05 and the cooling-rate correction factors are 0.99 (FBW-1), 1.01 (FBW-2) and 0.99 (FBG) (Table 3). We note that the ATRM measurements were performed after palaeointensity experiments during which some magnetomineralogical changes have occurred. Thus,

A. LISE-PRONOVOST ET AL.



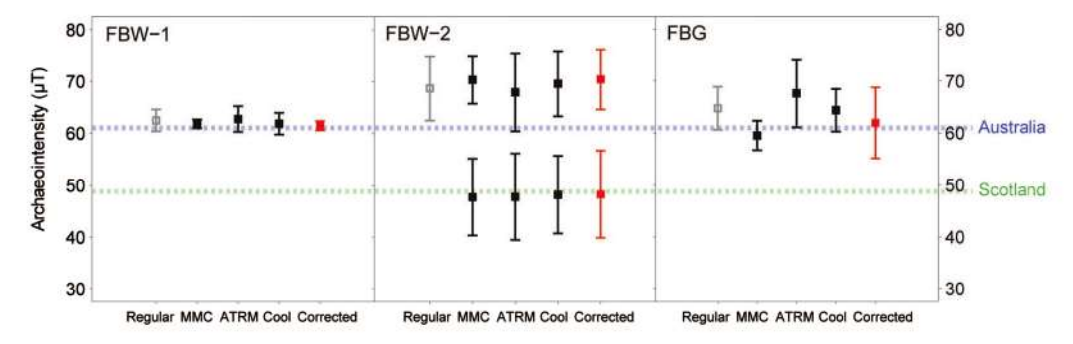


Fig. 8. Archaeointensity results per firebrick. The average archaeointensity value and standard deviation are shown before (regular: open symbol) and after corrections (corrected: in red), as well as for each individual correction, including the magnetomineralogical change (MMC), magnetic anisotropy (ATRM), and cooling-rate (cool) corrections. The horizontal lines indicate the average field intensity for East Lothian (48.79 μT) and Melbourne (61.02 μT) for the period 1842–1864 (gufm1 model: Jackson et al. 2000; https://www.ngdc.noaa.gov/geomag-web/?model=igrf#igrfwmm). Each brick has a vector component M2 acquired in Australia, and FBW-2 also has a vector component pM1 presumably acquired in Scotland. Note that the ATRM and cool corrections of FBW-2 pM1 are calculated from the MMC-corrected archaeointensity because the regular archaeointensities are class C (cf. Table 2).

magnetomineralogical changes may have impacted the anisotropy pre- and post-archaeointensity experiment. Nevertheless, the ATRM results for the fresh FBW samples are not distinct from the postarchaeointensity experiment samples, and observations of the bricks fabric from thin-section imaging (Fig. 2) indicate no visible preferred orientation. The average full-corrected archaeointensity values for MMC, ATRM and cool are $61.45 \pm 0.89 \,\mu\text{T}$ (FBW-1: six samples), $70.43 \pm 5.81 \,\mu\text{T}$ (FBW-2: six samples) and 61.92 \pm 6.84 μ T (FBG: five samples) (Table 3; Fig. 8). The archaeointensity values before and after corrections for FBW-1 and FBG overlap within uncertainties. The values before and after corrections also overlap for brick FBW-2; however, it has a higher average archaeointensity and standard deviation than the two other bricks.

The archaeointensity experiment results for the high-temperature vectors pM1 (Fig. 3) presumably acquired in Scotland are reported in Table 2. They are all class C and do not provide reliable archaeointensity estimates because of the small remanence fraction (f: Table 2) and magnetomineralogical alteration at high temperatures (d(pal) and d(CK): Table 2). However, applying the correction of Valet *et al.* (1996) upgrades three out of the four samples from brick FBW-2 to classes A and B, and an archaeointensity of $47.74 \pm 7.39 \,\mu\text{T}$ is estimated (Table 2; Fig. 7). Three samples out of six represent a success rate of 50%. The archaeointensity value after anisotropy and cooling-rate corrections is $48.30 \pm 8.39 \,\mu\text{T}$ (Table 3; Fig. 8).

Discussion

Local magnetic field contamination and insights into brick use

Despite FBW-1 and FBW-2 having the same manufacture history and magnetic mineralogy (Figs 4-6), brick FBW-2 has a higher average archaeointensity and larger standard deviation than the other bricks and the expected value for Australia during this period (61.17 \pm 0.078 μ T: Fig. 8). Furthermore, FBW-2 has a cross-brick transect from low to high archaeointensities (c. 65 µT on one side for samples C4 and C5 to $>73 \mu T$ on the other side for samples B1 and C1: Table 1). The magnetic analysis revealed no such trend in magnetic mineralogy, and the archaeointensity experiments are of the highest quality (class A: Table 1). Therefore, FBW-2 was likely to have been exposed to a contaminating magnetic field in the iron foundry at the time it last cooled down (e.g. fields produced via ironworking). If this were the case, then it can be further inferred that the source of magnetic field bias was located on the side of FBW-2 exposed to relatively lower temperatures: for example, higher archaeointensities are recorded on the side with double-vector components. These results highlight potential issues of contamination by non-Earth magnetic fields at archaeometallurgical sites, and further demonstrate the potential for using such magnetic analyses to help understand the context in which artefacts were used.

Fig. 7. Orthogonal projection and Arai plot for representative samples of bricks (a) FBW-1 with double-vector components M2 and pM1, (b) FBW-2 with double-vector components M2 and pM1, and (c) FBG with a single-component M2. The regular and MMC-corrected Arai plot and associated relative paleaointensity estimates are shown (ThellierTool: Leonhardt et al. 2004a).

Table 3. Archaeointensity results for successful specimens (classes A and B after MMC correction)

Brick	Sample	Archaeointensity (μT)								
		Regular	MMC-corrected	FATRM	ATRM-corrected	cool-corrected	Corrected			
FBW-1	A1	61.92	61.46	1.00	61.73	61.30	60.66			
	A4-M2	66.41	61.50	1.01	67.07	65.75	61.49			
	C4-M2	63.13	63.22	1.00	62.88	62.50	62.34			
	C5	61.16	60.70	1.03	63.18	60.55	62.08			
	D4	61.49	62.15	1.01	61.98	60.88	62.02			
	D5	60.63	61.83	0.98	59.54	60.02	60.11			
	Average	62.46	61.81		62.73	61.83	61.45			
	SD	2.11	0.84		2.48	2.09	0.89			
FBW-2	B1-M2	75.46	73.94	1.028	77.57	76.44	77.00			
	B2-M2	72.02	74.19	0.981	70.65	72.96	73.73			
	C1-M2	73.50	74.70	0.978	71.88	74.46	74.01			
	C2-M2	68.41	69.47	0.991	67.79	69.30	69.74			
	C4	59.56	64.46	0.932	55.51	60.33	60.86			
	C5	63.23	65.36	1.016	64.24	64.05	67.27			
	Average	68.70	70.35		67.94	69.59	70.43			
	SD	6.22	4.62		7.54	6.30	5.81			
	B1-pM1	NA	54.71	1.028	56.24	55.26	56.80			
	B2-pM1	NA	48.52	0.981	47.60	49.01	48.07			
	C2-pM1	NA	39.99	0.991	39.63	40.39	40.03			
	Average		47.74		47.82	48.22	48.30			
	SD		7.39		8.31	7.46	8.39			
FBG	C1*	NA	78.69	0.998	NA	NA	78.06			
	C2	60.55	56.22	1.069	64.73	60.19	59.74			
	C3	61.06	60.93	1.110	67.78	60.69	67.23			
	C4	69.38	63.53	1.113	77.22	68.96	70.28			
	C5	68.68	59.12	1.007	69.16	68.27	59.18			
	D1	64.05	57.76	0.926	59.31	63.67	53.16			
	Average	64.74	59.51		67.64	64.36	61.92			
	SD	4.14	2.84		6.56	4.12	6.84			

The archaeointensity value is provided for all corrections combined (corrected), and for each correction individually, including the magnetomineral change (MMC), the anisotropy of thermal remanent magnetization (ATRM) and the cooling-rate (cool) corrections. FATRM is the correction factor for anisotropy of the thermoremanent magnetization.

Potential for artefact sourcing using archaeointensities

Another result with potential applications in archaeology is the double archaeointensity record held by the firebricks (Figs 3 & 5). Despite poorly defined archaeointensities in the high-temperature component pM1 because of the small remanence fraction left and the more frequent alterations at high temperatures (Figs 4, 5 & 7), an average archaeointensity of 48.3 \pm 8.39 μT was calculated for class A and B samples of FBW-2 after corrections for magnetomineralogical changes, magnetic anisotropy and cooling rate (three samples: Table 2). This result is significantly lower than the historical field intensity in Melbourne and is consistent with the firebrick's manufacture in East Lothian, Scotland, where the magnetic field intensity is 48.62 μT for the period

1860-64 (according to the gufm1 model: https:// www.ngdc.noaa.gov/geomag/calculators/magcalc. shtml?model=igrf#igrfwmm), this brick having been produced post-1860 and used prior to 1864. This value is also consistent with archaeointensity values (48.8 \pm 1.10 μ T) for 1800-70 burnt sandstone from the Bolsterstone glassworks near Sheffield in the UK (Suttie 2010). Whilst in the current study the brick stamps clearly confirm their place of origin, in many cases the original provenance of archaeological materials is not clearly known, requiring sourcing analyses such as via X-ray fluorescence. For the archaeointensity-based method to be useful, the item in question needs to have acquired and preserved a TRM at its place of origin. If any secondary heating took place post-import, such as the present firebrick sample, the temperatures experienced must be low enough not to have completely

^{*}Significantly higher PI value. Not used in the average and standard deviation (SD) calculations.

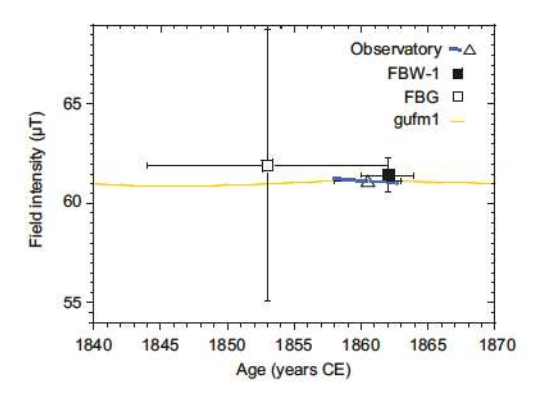


Fig. 9. Firebricks FBW-1 and FBG palaeointensity result and Melbourne observatory data compared with the model gufml (Jackson *et al.* 2000). Data from the observatory are represented by dashed lines for the monthly average and a symbol with error bars for the average value.

overprinted the original TRM. Such factors need to be taken into account when sampling: for example, being sure to take bricks away from the main source of secondary heat. A similar principle has been used to identify heat-treated silcrete stone artefacts in the archeological record stretching back to at least 72 ka (Brown *et al.* 2009). A further requirement is that past field intensities in the two locations must be known and unambiguously different (e.g. present-day South Africa at *c.* 25–29 μT and Victoria, Australia at *c.* 59–60 μT).

Archaeointensity and magnetic observatory data in Melbourne

The firebricks FBW-1 and FBG provide archaeointensity results that overlap with the gufm1 historical model for Australia over the period 1842-64, based on mariners' data (Jackson et al. 2000) (Fig. 8; Table 1). The Melbourne archaeointensity data also overlap with the Melbourne magnetic observatory data (Fig. 9). There is a close fit in age and intensity between the archaeointensity from FBW-1 (1860-64: $61.45 \pm 0.89 \,\mu\text{T}$) and the direct monthly measurement averaged over 5 years (from January 1858 to February 1863: $61.17 \pm 0.078 \,\mu\text{T}$). Figure 10 presents the Melbourne archaeointensity data in the context of the available SE Australia late Holocene data (last 3 ka) and model outputs for Melbourne in the GEOMAGIA database. Models CALS3k.4 and SED3k.1 are based on the gufm1 model for the last 400 years and thus return a good fit (Fig. 10). In contrast, the models that are not constrained by gufm1 overestimate (pfm9k: Nilsson et al. 2014) or underestimate (HFM.O-L1.AL1: Panovska et al. 2015; Constable et al. 2016) mid-nineteenth-century palaeointensity in Melbourne. While HFM.OL1.AL1 underestimates the historical gufm1 model, it plots within the uncertainty of FBG (1842-64: $61.92 \pm 6.84 \,\mu\text{T}$). The poorly defined centennial- to millennial-scale magnetic field variability in SE Australia is further reflected by model outputs differing by up to 12 µT with an average difference of $6.1 \pm 2.4 \,\mu\text{T}$ (over

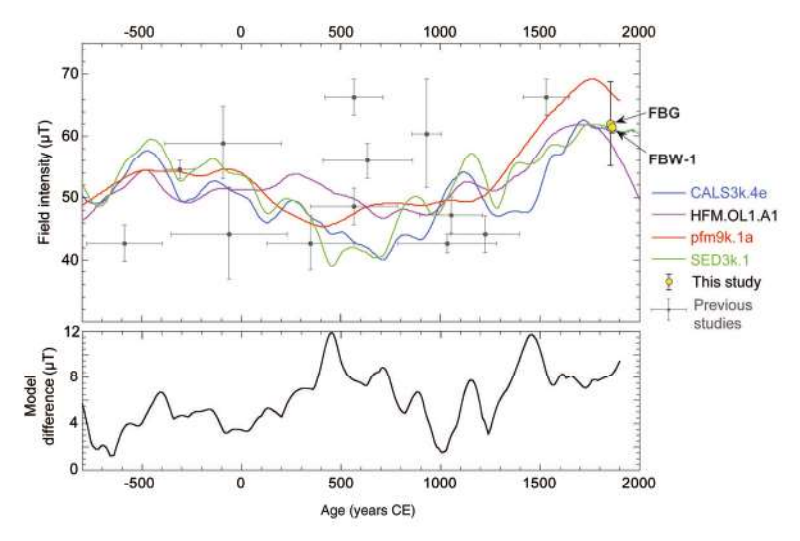


Fig. 10. The firebrick archaeointensity data from Melbourne compared to geomagnetic field models outputs for Melbourne (SED3k.1, Korte et al. 2009; CALS3k.4, Korte & Constable 2011; pfm9k, Nilsson et al. 2014; HFM.OL1.AL1, Panovska et al. 2015; Constable et al. 2016) and the available Australian archaeointensity data (Barbetti et al. 1983) in the GEOMAGIA database (Brown et al. 2015). The lower panel is the intensity difference between models outputs for the period –800 to 1900 CE.

the period -800 to 1900 CE: Fig. 10), large scatter, and large age and intensity uncertainties of the archaeomagnetic dataset (up to ± 292 years and $\pm 8.8~\mu T$) (Fig. 10). The closest palaeointensity outside Australia during the nineteenth century is also consistent with this study and is from the North Island of New Zealand, where the Tarawera basalt dyke (38.22° S, 176.52° E) from the 1886 CE eruption provides a palaeointensity value of 62.9 \pm 5.7 μT (Tanaka $\it et al.$ 2009). The new Melbourne archaeointensity data are the most precisely dated archaeomagnetic data in Australia, with an age uncertainty of ± 2 and ± 9 years for FBW-1 and FBG, respectively (Fig. 10).

Conclusion

The first historical archaeomagnetic intensity study in Australia was conducted on well-dated mid-nineteenth-century Scottish firebricks. The three studied bricks (FBW-1, FBW-2 and FBG) have a high (94%) archaeointensity experiment success rate, and two bricks (FBW-1 and FBG) provide archaeointensities in agreement with absolute magnetic field intensity measurements performed at the same time and place, and with the historical model gufm1 (Jackson et al. 2000). More palaeomagnetic and archaeomagnetic data of this type are required from Australia to document the regional magnetic field behaviour in this under-documented region of the globe. The two bricks from the same manufacturer 'John Grieve Bank Park Firebrick Works' (FBW-1 and (FBW -2) have a similar magnetic mineralogy and were apparently exposed to lower temperatures than the third brick (FBG) because they retain a high-temperature magnetic vector component (pM1), presumably acquired during the initial firing fabrication in Scotland. Despite a low (50%) success rate, the pM1 archaeointensity is in agreement with the magnetic field in Scotland at the time. This methodology has the potential to answer questions about the origin of other fired technology where there are questions over whether it was manufactured locally or imported. Finally, one brick (FBW-2) overestimates the expected field values for Australia, suggesting brick usage in the iron foundry somewhere near a local magnetic field at the time of the brick's last cooling. This work demonstrates the potential of using archaeointensity methods for artefact sourcing and artefact usage investigations; a good addition to the toolkit of magnetic sourcing techniques for archaeology (e.g. Frahm & Feinberg 2013).

Acknowledgements Thanks to Sarah Myers of ArchLink Archaeologists and Heritage Advisors P/L, along with Jeremy Smith and Anne-Louise Muir of

Heritage Victoria for access to the iron foundry site and materials. We acknowledge the Geoscience Australia Geomagnetism Section and Adrian Hitchman for collaboration and interpretation of the Melbourne observatory data. Thanks to Mike Jackson, Dario Bilardello and the Institute for Rock Magnetism (IRM) team at the University of Minneapolis, and Andrew Roberts, Xiang Zhao and the Paleomagnetism Laboratory team at the Australian National University for access to VSM and support with cooling-rate experiments.

Funding This work is supported by a La Trobe University Postgraduate Research Scholarship and IRM Visiting Research Fellowship (funded through the US National Science Foundation) to T. Mallett, and a La Trobe University Research Fellowship and a Postdoctoral Fellowship of Fonds Nature et Technologies – Gouvernement du Quebec (FQNRT) to A. Lise-Pronovost.

Author contributions AL-P: conceptualization (equal), formal analysis (lead), funding acquisition (lead), investigation (equal), methodology (lead), writing – original draft (equal); TM: conceptualization (equal), formal analysis (equal), funding acquisition (equal), investigation (equal), methodology (supporting), writing – original draft (equal), funding acquisition (equal), formal analysis (equal), funding acquisition (equal), methodology (supporting), supervision (lead), writing – review & editing (equal).

References

- ANKER, S.A., COLHOUN, E.A., BARTON, C.E., PETERSON, M. & BARBETTI, M. 2001. Holocene vegetation and paleoclimatic and paleomagnetic history from Lake Johnston, Tasmania. *Quaternary Research*, 56, 264–274, https://doi.org/10.1006/qres.2001.2233
- BARBETTI, M. 1973. Archaeomagnetic and Radiocarbon Studies of Aboriginal Fireplaces. PhD thesis, Australian National University.
- BARBETTI, M. 1977. Measurements of recent geomagnetic secular variation in southeastern Australia and the question of dipole wobble. *Earth and Planetary Science Letters*, **36**, 207–218, https://doi.org/10.1016/0012-821X(77)90200-X
- BARBETTI, M. & McElhinny, M. 1972. Evidence of a geomagnetic excursion 30 000 yr BP. *Nature*, 239, 327–330, https://doi.org/10.1038/239327a0
- BARBETTI, M. & MCELHINNY, M. 1976. The Lake Mungo geomagnetic excursion. *Philosophical Transactions of the Royal Society of London Series A: Mathematical and Physical Sciences*, 281(1305), https://doi.org/10. 1098/rsta.1976.0048
- BARBETTI, M., McElhinny, M.W., Edwards, D.J. & Schmidt, P.W. 1983. Archeomagnetic results from Australia. In: Creer, K.M., Tucholka, P. & Barton, C.E. (eds) Geomagnetism of Baked Clays and Recent Sediments. Elsevier, Amsterdam, 173–175.
- BARTON, C.E. & McEl-HINNY, M. 1981. A 10 000 yr geomagnetic secular variation record from three Australian maars. Geophysical Journal International, 67,

- 465–485, https://doi.org/10.1111/j.1365-246X.1981.tb02761.x
- BARTON, C.E. & BARBETTI, M. 1982. Geomagnetic secular variation from recent lake sediments, ancient fireplaces and historical measurements in southeastern Australia. *Earth and Planetary Science Letters*, 59, 375–387, https://doi.org/10.1016/0012-821X(82)90139-X
- BOWLER, J.M., JOHNSTON, H., OLLEY, J.M., PRESCOTT, J.R., ROBERTS, R.G., SHAWCROSS, W. & SPOONER, N.A. 2003. New ages for human occupation and climatic change at Lake Mungo, Australia. *Nature*, 421, 837–840, https://doi.org/10.1038/nature01383
- BROWN, M.C., DONADINI, F. ET AL. 2015. GEOMA-GIA50.v3: 1. General structure and modifications to the archeological and volcanic database. Earth, Planets and Space, 67, 83, https://doi.org/10.1186/s40623-015-0232-0
- Brown, K.S., Marean, C.W. et al. 2009. Fire as an engineering tool of early modern humans. Science, 325, 859–862, https://doi.org/10.1126/science.1175028
- CHAUVIN, A., GARCIA, Y., LANOS, P. & LAUBENHEIMER, F. 2000. Paleointensity of the geomagnetic field recovered on archaeomagnetic sites from France. *Physics of the Earth and Planetary Interiors*, 120, 111–136, https:// doi.org/10.1016/S0031-9201(00)00148-5
- CLARK, P.M. & BARBETTI, M. 1982. Fires, hearths and palaeomagnetism. *In*: AMBROSE, W. & DUERDEN, P. (eds) *Archaeometry: An Australasian Perspective*. Canberra, Department of Prehistory, Australian National University, 144–150.
- CLARKSON, C., JACOBS, Z. ET AL. 2017. Human occupation of northern Australia by 65 000 years ago. Nature, 547, 306–310, https://doi.org/10.1038/nature22968
- COE, R.S. 1967. Paleo-intensities of the Earth's magnetic field determined from tertiary and quaternary rocks. *Journal of Geophysical Research*, 72, 3247–3262, https://doi.org/10.1029/JZ072i012p03247
- CONSTABLE, C.G. 1985. Eastern Australian geomagnetic field intensity over the past 14 000 yr. Geophysical Journal of the Royal Astronomical Society, 81, 121–130, https://doi.org/10.1111/j.1365-246X.1985.tb01354.x
- CONSTABLE, C.G. & MCELHINNY, M.W. 1985. Holocene geomagnetic secular variaton records from northeastern Australian lake sediments. Geophysical Journal of the Royal Astronomical Society, 81, 103–120, https://doi.org/10.1111/j.1365-246X.1985.tb01353.x
- CONSTABLE, C.G., KORTE, M. & PANOVSKA, S. 2016. Persistent high paleosecular variation activity in southern hemisphere for at least 10 000 years. Earth and Planetary Science Letters, 453, 78–86, https://doi.org/10.1016/j.epsl.2016.08.015
- DOUGLASS, G. & OGLETHORPE, M. 1993. Brick, Tile and Fireclay Industries in Scotland. Royal Commission on the Ancient and Historical Monuments of Scotland, Edinburgh, UK.
- DOUGLAS, G.J., HUME, J.R., MOIR, L. & OGLETHORPE, M.K. 1985. A Survey of Scottish Brickmarks. Scottish Industrial Archaeology Survey, University of Strathclyde, Glasgow, UK.
- DUNLOP, D.J. & ÖZDEMIR, Ö. 1997. Rock Magnetism, Fundamental and Frontiers. Cambridge University Press, New York.
- EGLI, R. 2013. VARIFORC: an optimized protocol for calculating non-regular first-order reversal curve

- (FORC) diagrams. Global and Planetary Change, 110, 302–320, https://doi.org/10.1016/j.gloplacha. 2013.08.003
- FRAHM, E. & FEINBERG, J.M. 2013. From flow to quarry: magnetic properties of obsidian and changing the scale of archaeological sourcing. *Journal of Archaeological Science*, 40, 3706–3721, https://doi.org/10. 1016/j.jas.2013.04.029
- Fox, J.M.W. & AITKEN, M.J. 1980. Cooling rate dependance of the thermoremanent Magnetization. *Nature*, 283, 462–463, https://doi.org/10.1038/283462a0
- GALE, S.J., COOK, D. & DORRINGTON, N.J. 2013. The eastern Australian magnetic inclination record: dating the recent past and re-assessing the historical geomagnetic archive. *The Holocene*, 23, 398–415, https://doi.org/ 10.1177/0959683612463094
- GAUSS, C.F. 1833. Intensitas vis magneticae terrestris ad mensuram absolutam revocata. Goettingen Gesellschaft der Wissenschaften, 8, 3–44.
- GENEVEY, A. & GALLET, Y. 2002. Intensity of the geomagnetic field in western Europe over the past 2000 years: New data from ancient French pottery. *Journal of Geophysical Research*, B11, 2285, https://doi.org/10.1029/2001JB000701
- GENEVEY, A., GALLET, Y., CONSTABLE, C.G., KORTE, M. & HULOT, G. 2008. ArcheoInt: an upgraded compilation of geomagnetic field intensity data for the past ten millennia and its application to the recovery of the past dipole moment. *Geochemistry*, *Geophysics*, *Geosystems*, 9, Q04038, https://doi.org/10.1029/2007/GC001881
- GOGUITCHAICHVILI, A., MORALES, J., SCHAVELZON, D., VÁS-QUEZ, C., GOGORZA, C.S.G., LOPONTE, D. & RAPALINI, A. 2015. Variations of the Earth's magnetic field strength in South America during the last two millennia: New results from historical buildings of Buenos Aires and re-evaluation of regional data. *Physics of the Earth and Planetary Interiors*, 245, 15–25, https:// doi.org/10.1016/j.pepi.2015.05.006
- Gómez-Paccard, M., Chauvin, A. et al. 2019. New archeointensity data from NW Argentina (1300–1500 CE), Physics of the Earth and Planetary Interiors 286, 92–100. https://doi.org/10.1016/j.pepi.2018.11.004
- HARE, V.J., TARDUNO, J.A. Et Al. 2018. New archeomagnetic directional records from iron age Southern Africa (ca. 425–1550 CE) and implications for the South Atlantic anomaly. Geophys Res Lett, 45, 1361–1369.
- HARRISON, R.J. & FEINBERG, J.M. 2008. FOR Cinel: an improved algorithm for calculating first-order reversal curve distributions using locally weighted regression smoothing. *Geochemistry, Geophysics, Geosystems*, 9, Q05016, https://doi.org/10.1029/2008GC001987
- HARTMANN, G.A., GENEVEY, A., GALLET, Y., TRINDADE, R.I.F., ETCHEVARNE, C., LE GOFF, M. & AFONSO, M. 2010. Archeointensity in Northeast Brazil over the past five centuries. Earth and Planetary Science Letters, 296, 340–352, https://doi.org/10.1016/j.epsl.2010.05.016
- HERVÉ, G., CHAUVIN, A., LANOS, P., ROCHETTE, P., PERRIN, M. & PERRON D'ARC, M. 2019. Cooling rate effect on thermoremanent magnetization in archaeological baked clays: an experimental study on modern bricks. Geophysical Journal International, 217, 1413–1424, https://doi.org/10.1093/gji/ggz076
- HIGHLEY, D.E. 1982. Geological distribution, exploitation and utilization of fireclays from the United Kingdom.

- Transactions of the Institution of Mining and Metallurgy, 91, 11–16.
- JACKSON, A., JONKERS, A.R.T. & WALKER, M.R. 2000. Four centuries of geomagnetic secular variation from historical records. *Philosophical Transactions of the Royal Society A: Mathematical, Physical and Engineering Sciences*, 358, 957–999, https://doi.org/10.1098/ rsta.2000.0569
- KORTE, M. & CONSTABLE, C. 2011. Improving geomagnetic field reconstructions for 0–3 ka. *Physics of the Earth* and *Planetary Interiors*, 188, 247–259, https://doi. org/10.1016/j.pepi.2011.06.017
- KORTE, M., DONADINI, F. & CONSTABLE, C.G. 2009. Geomagnetic field for 0–3 ka: 2. A new series of time-varying global models. Geochemistry, Geophysics, Geosystems, 10, Q06008, https://doi.org/10.1029/2008GC002297
- LAJ, C. & CHANNELL, J.E.T. 2015. Geomagnetic excursions. In: Kono, M. (ed.) Geomagnetism. Treatise on Geophysics, 5. Elsevier, Amsterdam, 373–416.
- LEONHARDT, R., HEUNEMANN, C. & KRÁSA, D. 2004a. Analyzing absolute paleointensity determinations: Acceptance criteria and the software ThellierTool4.0. Geochemistry, Geophysics, Geosystems, 5, Q12016, https://doi.org/10.1029/2004GC000807
- LEONHARDT, R., KRASA, D. & COE, R.S. 2004b. Multidomain behavior during Thellier paleointensity experiments: a phenomenological model, *Physics of the Earth and. Planetary Interiors*, 147, 127–140, https://doi.org/10.1016/j.pepi.2004.01.009
- LISÉ-PRONOVOST, A., MALLETT, T., MYERS, S., ANDERSON, W., MUIR, A.-L. & HERRIES, A.I.R. 2016. Understanding the life history of 19th-century Australian bricks using archaeomagnetism and the establishment of a south-east Australian archaeomagnetic dating reference curve (SEAARC). In: SPRY, C., FOLEY, E., FRANKEL, D. & LAWRENCE, S. (eds) Excavations, Surveys and Heritage Management in Victoria, Volume 5. La Trobe University, Melbourne, Australia, 57–67.
- LÓPEZ-SANCHEZ, J., MCINTOSH, G. ET AL. 2017. Epsilon iron oxide: origin of the high coercivity stable low Curie temperature magnetic phase found in heated archeological materials. Geochemistry, Geophysics, Geosystems, 18, 2646–2656, http://doi.org/10.1002/ 2017GC006929
- LURCOCK, P.C. & WILSON, G.S. 2012. PuffinPlot: a versatile, user-friendly program for paleomagnetic analysis. Geochemistry, Geophysics, Geosystems, 13, Q06Z45, https://doi.org/10.1029/2012GC004098
- MALLETT, T., MYERS, S., MIRAMS, S., COLEMAN, F. & SHANA-HAN, F. 2015. Preliminary results of excavations at Langlands Iron Foundry and Stooke's Shipping Butchers, 556–560 Flinders Street, Melbourne. In: SPRY, C., FRANKEL, D. & LAWRENCE, S. (eds) Excavations, Surveys and Heritage Management in Victoria, Volume 4. La Trobe University, Melbourne, Australia, 85–92.
- MAXBAUER, D., FEINBERG, J. & Fox, D.L. 2016. MAX UnMix: a web application for unmixing magnetic coercivity distributions. *Computers & Geosciences*, 95, 140–145, https://doi.org/10.1016/j.cageo.2016. 07.009
- MYERS, S., MIRAMS, S. & MALLETT, T. 2018. Langlands iron foundry, flinders street, Melbourne. *International Journal of Historical Archaeology*, 22, 78–99, https://doi.org/10.1007/s10761-017-0417-2

- Neumayer, G. 1867. Discussion of the Meteorological and Magnetical Observations made at the Flagstaff Observatory, Melbourne, during the years 1858–1863 by Georg Neumayer. J. Schneider, Mannheim, Germany, https://babel.hathitrust.org/cgi/pt?id=nyp.334330908 99141;view=1up;seq=5
- NEUKIRCH, L., TARDUNO, J., HUFFMAN, T., WATKEYS, M., SCRIBNER, C.A. & COTTRELL, R. 2012. An archeomagnetic analysis of burnt grain bin floors from ca. 1200 to 1250 AD Iron-Age South Africa. *Physics of the Earth and Planetary Interiors*, 190, 71–79, https:// doi.org/10.1016/j.pepi.2011.11.004
- NILSSON, A., HOLME, R., KORTE, M., SUTTIE, N. & HILL, M. 2014. Reconstructing Holocene geomagnetic field variation: new methods, models and implications. Geophysical Journal International, 198, 229–248, https:// doi.org/10.1093/gji/ggu120
- PANOVSKA, S., KORTE, M., FINLAY, C.C. & CONSTABLE, C.G. 2015. Limitations in paleomagnetic data and modelling techniques and their impact on Holocene geomagnetic field models. *Geophysical Journal International*, 202, 402–418, https://doi.org/10.1093/gji/ ggv137
- POLETTI, W., TRINDADE, R.I.F., HARTMANN, G.A., DAMIANI, N. & RECH, R.M. 2016. Archeomagnetism of Jesuit Missions in South Brazil (1657–1706 AD) and assessment of the South American database. Earth and Planetary Science Letters, 445, 36–47, https://doi.org/10. 1016/j.epsl.2016.04.006
- POLETTI, W., BIGGIN, A.J., TRINDADE, R.I.F., HARTMANN, G.A. & TERRA-NOVA, F. 2018. Continuous millennial decrease of the Earth's magnetic axial dipole, Physics of the Earth and Planetary Interiors. 274, 72–86, https://doi.org/10.1016/j.pepi.2017.11.005
- RIISAGER, P. & RIISAGER, J. 2001. Detecting multidomain magnetic grains in Thellier paleointensity experiments, Physics of the Earth and Planetary Interiors, 125, 111–117, https://doi.org/10.1016/S0031-9201(01) 00236-9
- ROBERTS, A.P. 2008. Geomagnetic excursions: knowns and unknowns. Geophysical Research Letters, 35, L17307.
- ROBERTS, A.P., HESLOP, D., ZHAO, X. & PIKE, C.R. 2014. Understanding fine magnetic particle systems through use of first-order reversal curve diagrams. *Reviews of Geophysics*, 52, 557–602, https://doi.org/10.1002/ 2014RG000462
- ROGERS, J., FOX, J. & AITKEN, M.J. 1979. Magnetic anisotropy in ancient pottery. *Nature*. 277. 644–646. https://doi.org/10.1038/277644a0
- SANDERSON, K.W. 1990. The Scottish Refractory Industry, 1830–1980. Redwood Press Limited, Melksham, Wiltshire, UK.
- SINGER, B. 2014. A Quaternary geomagnetic instability time scale. *Quaternary Geochronology*, 21, 29–52, https:// doi.org/10.1016/j.quageo.2013.10.003
- SUTTIE, N.A. 2010. Geomagnetic Field Archaeointensities from Britain and the Application of the Microwave Palaeointensity Method to Materials of Differing Dielectric Properties. PhD thesis, University of Liverpool.
- TANAKA, H., KOMURO, N. & TURNER, G.M. 2009. Palaeosecular variation for 0.1–21 Ka from the Okataina Volcanic Centre, New Zealand. Earth, Planets and Space, 61, 213–225, https://doi.org/10.1186/BF0 3352901

- TARDUNO, J., WATKEYS, M. ET AL. 2015. Antiquity of the South Atlantic Anomaly and evidence for top-down control on the geodynamo. *Nature Communications*, 6, 7865, https://doi.org/10.1038/ncomms8865
- TEMA, E., CAMPS, P., FERRARA, E. & POIDRAS, T. 2015. Directional results and absolute archaeointensity determination by the classical Thellier and the multi-specimen DSC protocols for two kilns excavated at Osterietta, Italy. Studia Geophysica et Geodaetica, 59, 554–577, https://doi.org/10.1007/s11200-015-0413-0
- THELLIER, O. & THELLIER, E. 1959. Sur la direction du champ magnetique terrestre dans le passe historique et geologique. Annales de Geophysique, 15, 285–375.
- VALET, J.-P., BRASSART, J., LE MEUR, I., SOLER, V., QUIDELLEUR, X., TRIC, E. & GILLOT, P.-Y. 1996. Absolute paleointensity and magnetomineralogical changes.

- Journal of Geophysical Research, 1012, 25 029–25 044, https://doi.org/10.1029/96JB02115
- VEITCH, R.J., HEDLEY, I.G. & WAGNER, J.J. 1984. An investigation of the intensity of the geomagnetic field during Roman times using magnetically anisotropic bricks and tiles. Archives des sciences et compte rendu des séances de la Société, 37, 359–373.
- YU, Y. & DUNLOP, D.J. 2002. Multivectorial paleointensity determination from the Cordova Gabbro, southern Ontario. Earth and Planetary Science Letters, 203, 983–998, https://doi.org/10.1016/S0012-821X(02) 00900-7
- Yu, Y.J. & TAUXE, L. 2005. Testing the IZZI protocol of geomagnetic field intensity determination. *Geochemistry, Geophysics, Geosystems*, 6, Q05H17, https://doi. org/10.1029/2004GC000840